

Black Cool Pigments for Urban Heat Island (UHI) Control: from Cr-Hematite to Mn-Melilite

G. Monrós*, S. Cerro, J.A. Badenes and M. Llusar

Dpt. Of Inorganic and Organic Chemistry, Jaume I University, 12070 Castelló, Spain

Abstract: Black cool pigments are very interesting for its application in asphalt urban pavements and building floors for moderate the urban heat island effect (UHI) and improving air conditioning energy efficiency. Cool black pigments based on Cr doped hematite Fe_2O_3 (trigonal, $R\text{-}3c$), hexagonal perovskites YMnO_3 (hexagonal, $P6_3cm$) and $\text{Sr}_4\text{CuMn}_2\text{O}_9$ (trigonal, $P321$) and melilite $\text{Sr}_2(\text{Mg}_{0.5}\text{Mn}_{0.5})\text{Ge}_2\text{O}_7$ (tetragonal, $P\text{-}42_1m$) with high NIR reflectance synthesized by ceramic and coprecipitation method, are analyzed and compared from color yield in alkyd paint, ceramic glazes and porcelain stoneware, NIR reflectance, bandgap and photocatalytic activity on Orange II substrate. $\text{Sr}_4\text{CuMn}_2\text{O}_9$ black powders show the nearest hue h to the reference carbon black and the highest NIR reflectance (51%). All pigments show high NIR reflectance in all tested applications. The $\text{Fe}_{1.2}\text{Cr}_{0.8}\text{O}_3$ pigment shows good behavior in the free ZnO glaze and also in porcelain stoneware, YMnO_3 and $\text{Sr}_4\text{CuMn}_2\text{O}_9$ pigments are compatible with low temperature glazes, but $\text{Sr}_2(\text{Mg}_{0.5}\text{Mn}_{0.5})\text{Ge}_2\text{O}_7$ pigment loses the black color even in low temperature glazes. $\text{Sr}_4\text{CuMn}_2\text{O}_9$ pigment shows moderate photoactivity on Orange II ($t_{1/2}=216$ min) and the $\text{Fe}_{1.2}\text{Cr}_{0.8}\text{O}_3$ pigment also shows some activity ($t_{1/2}=329$ min).

Keywords: Black pigment, Cool pigment, Urban heat island, Photocatalysis, Glazes.

1. INTRODUCTION

Buildings are responsible of about the 36% of primary energy consumption and 30% of greenhouse gas emissions in U.S. Therefore, strategies such as Leadership in Energy and Environmental Design (LEED) certification, promoted by the U.S. Green Building Council, analyze the sustainability of buildings considering factors associated with their design and construction such as the content of recycled material in their composition, the use of regional raw materials for their manufacture, innovation and design (functionality) and the urban heat island effect (UHI). Regarding the urban heat island effect, the determination of the Solar Reflectance Index (SRI) for opaque materials (wall, roof and floor) aids the LEED certification. SRI reveals the ability of a surface to reflect solar radiation and to emit thermal radiation, reducing the increase in temperature caused by the incidence of solar radiation on the surface. The SRI of a specific surface changes with the solar reflectance R and thermal emittance of the material, and also according to certain environmental conditions, such as the solar flux, the convection coefficient, the air temperature and the sky temperature (ASTM E1980 2011). In the case of roof tiles for buildings, the SRI value required for a specific material is dependent on the slope of the roof ($\text{SRI} \geq 39$ for steep slope; $\text{SRI} \geq 82$ for low slope) [1].

The so-called eco-friendly cool pigments are being studied in recent years can be defined as a pigment with high coloring capacity in matrices such as paints, glass, ceramics, similar to a conventional one (and therefore with similar reflectance in the visible spectrum), but with high reflectance in the near infrared (NIR 750-2500 nm); so it reflects this radiation moderating the heating of the surface. Figure 1 shows the behavior of a conventional carbon black pigment compared to the Cr-hematite black pigment reported in this paper (A pigment) [1, 2].



Figure 1: Thermal behavior of the carbon black pigment and the black Cr-hematite (A pigment) (10 wt% added to alkyd paint) [1, 2].

The wooden plate closes the open ceiling of a 20x20x20 cm cement cube colored in white. When irradiated by the infrared lamp, the equilibrium temperature after several hours of irradiation indicates

*Address correspondence to this author at the Dpt. Of Inorganic and Organic Chemistry, Jaume I University, 12070 Castelló, Spain; Tel: 34964728250; E-mail: monros@uji.es

that inside the cabin closed with the wood colored with the Cr-hematite black pigment it is 32.3°C compared to 37.6°C in the cabin closed with the wood colored with carbon black. The reason for this behavior is described in Figure 2, which shows the reflectance spectra of both surfaces.

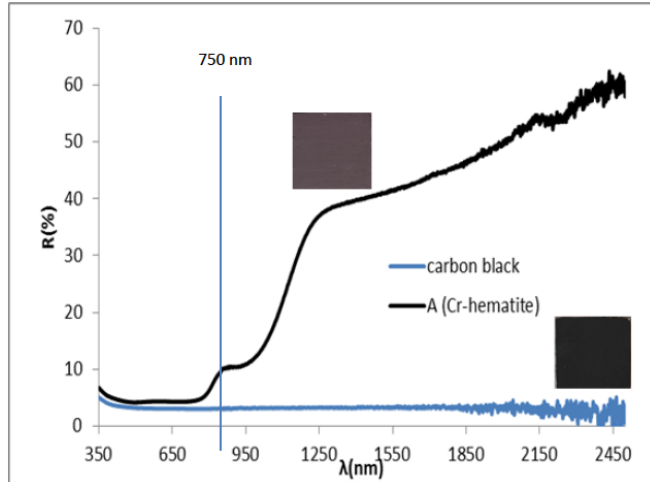


Figure 2: Reflectance spectra of the carbon black and black (A) Cr-hematite pigments 10 wt% added to alkyd paint applied over wood surface [1, 2].

The spectrum of the carbon black surface has a low reflectance R throughout the spectrum; in the visible area (300-750 nm). On the other hand, black plate has low reflectance in the visible range, but from 750 nm in the infrared range, it reflects around 36% of the radiation so that it heats up much less than carbon black that reflects practically nothing. In addition to the cooling effect on buildings, if they are used intensively, the use of cooling pigments has a global impact on terrestrial albedo and therefore on climate change, as described in Figure 3 [3, 4].

The snowy landscapes in Figure 3 show a reflectance to sunlight higher than 80%. This type of landscape gradually disappears in time and space due to the effect of climate change (e.g., polar caps regression). In forested areas the reflectivity, tempered by the humidity of the chlorophyll mass of the forest remains relatively high ($> 37\%$). However in deforested, anthropized and desertified areas, the reflectivity is always less than 5% using conventional asphalt. The effect of climate change and anthropization induces changes in the landscape towards the surfaces of $R = 2$, retreating the reflective forested and snowy areas, with which the warming worsens in a cyclical way. The reversal or moderation of the cycle can be achieved, among other methods, by

increasing the global reflectance using, for example, highly reflectance pigments in roads and insolated surfaces.

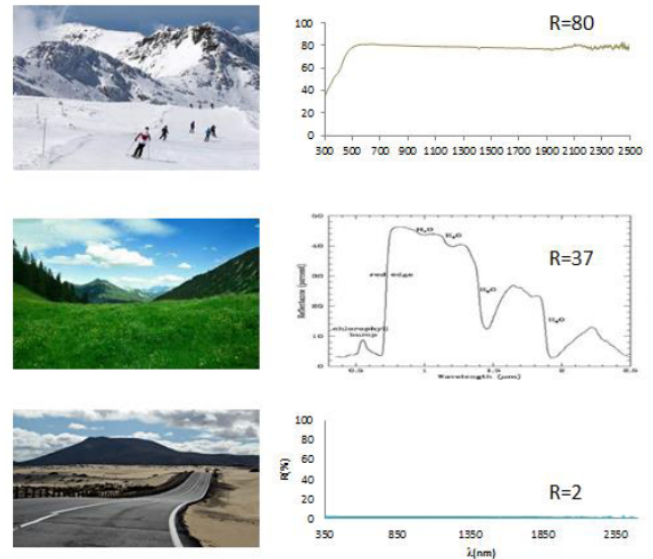


Figure 3: Reflectance $R(\%)$ of a surface; albedo effect and climate change [3, 4].

When using reflective surfaces that produce cooling of the surfaces, the normal and intuitive question about energy efficiency always appears: “if these pigments are used, it is clear that in summer we will save on air conditioning but, what happens in winter? Will we spend more on heating? The answer is that, in fact, in winter in periods of insolation a small portion of energy is lost by reflection, but the period of winter light is half that in summer and in temperate climates the period and energy of solar irradiation (W/m^2) are much lower and more the colder the climate, without forgetting that in cold climates the surfaces are stained white by frost and snow, so that our insolated pigments in snowy environments cool much less than the surface bleached by snow. In short, a rigorous life cycle analysis applied to any type of climate, from the hottest to the coldest, indicates that the use of highly reflective surfaces is always efficient [4], with efficiency much more evident in hot and temperate climates.

Following the Dry Color Manufacturers Association, pigment powders are classified in three categories [5, 6]:

- *Category A* deals with pigments suspended in glass matrixes which require the highest degree of heat stability and chemical resistance to withstand the attack of molten glass.

- *Category B* deals with pigments suspended in plastics and other polymers, which require only moderate heat stability.

- *Category C* deals with pigments suspended in liquid vehicles, which require little, or no heat stability.

In order to achieve cool pigments, several factors should be considered: (a) Absence of absorbent species in the NIR range (700-2500 nm.): e.g. Co^{2+} in tetrahedral environment shows a strong absorbance in the 1200-1600 nm (due to the coupling of d-d transitions bands ${}^4\text{A}_2(\text{F}) \rightarrow {}^4\text{T}_1(\text{F})$ at 1400 nm and ${}^4\text{A}_2(\text{F}) \rightarrow {}^4\text{T}_2(\text{F})$ at 1600 nm) which hinders its application as NIR reflector but there is no simple alternative for blue color in glazes [7]. In this sense, a good NIR reflector is a semiconductor with relatively high band gap such as TiO_2 (2.4 eV) or CdS, ZnO and SrTiO_3 (3.4 eV), with an intense charge transfer band located at UV range that block the UV radiation and protect the organic binders, (b) High thermal emittance. Thermal emittance is the measure of a material ability to release heat that it has absorbed and therefore its temperature is moderated [8]. The emittance index of solids is high (e.g. ceramics 0.9, asphalt 0.88) except in the case of conductive metals (e.g. Ag 0.02, Al 0.03, Cu 0.04) [1].

Obviously, a pigment should have high pigmentation yield when dispersed in the matrices (polymers, glass, ceramics...). For achieve high pigmentation capacity two factors are critical: (a) High refractive index that allows achieving high scattering efficiency of light when the pigment is added to a matrix with very different refractive index. The scattering efficiency increases with the difference of the refractive index pigment-medium. The polymorphs of TiO_2 anatase and rutile show high refractive index (2.55 and 2.73 respectively), then pigments based on rutile lattice such as ochre of Cr-Sb rutile or yellow of Ni-Sb rutile are two of the best classical cool pigments. Related pigments such as Cr-pseudobrookite ($\text{Cr-Fe}_2\text{TiO}_5$) [9], Cr-armalcolite ($\text{Cr-(MgFe}_2\text{Ti}_3\text{O}_5$) [10] or Ni-geikielite (Ni-MgTiO_3) [11] based on titanates also show high NIR reflectance, (b) Particle size should be about half the wavelength of the light, hence for NIR light (700-2500 nm) the particle diameter should be between 350-1250 nm. But it is important to note that a fine pigment with lower particle size shows higher surface area and number of particles, which probably compensates the low scattering of dissimilar size, and therefore it can show higher NIR reflectance. The particle shape and packing status are other important factors, in addition to the particle size. However, it is important to note that in

ceramic applications the particle size must reach a minimum value that resist the attack of the media: fine particles are solved by the glazes or ceramic stoneware [1].

Several of the published cool pigments are only evaluated in powder form and, sometimes, their lightness is outside Munsell's optimal chroma, resulting in pale colors [12-14]. Black cool pigments are very interesting for its application in asphalt urban pavements and building floors for moderate the urban heat island effect (UHI) and improving air conditioning energy efficiency. Cool black pigments based on Cr doped hematite Fe_2O_3 (trigonal, *R-3c*), hexagonal perovskites YMnO_3 (hexagonal, *P6₃cm*) and $\text{Sr}_4\text{CuMn}_2\text{O}_9$ (trigonal, *P321*) and melilite $\text{Sr}_2(\text{Mg}_{0.5}\text{Mn}_{0.5})\text{Ge}_2\text{O}_7$ (tetragonal, *P-42₁m*) with high NIR reflectance synthesized by ceramic and ammonia coprecipitation method, are analyzed and compared from color yield in ceramic glazes and ceramic stoneware, NIR reflectance, bandgap and photocatalytic activity on Orange II substrate.

2. EXPERIMENTAL

2.1. Samples Preparation

The classic black reference pigment is the carbon black based on graphite, but as described in Figure 2 its NIR reflectance is negligible. According to Akbary and Levinson [2] the classical black pigments with high NIR reflectance (measured in films of the order of 11-30 μm thick in PVC applications) are the inorganic black of Cr-hematite solid solution and also the organic Perylene black pigment that absorbs strongly in the visible and very weakly in the NIR (but unusable in ceramic matrices and its nature as PAH could induce negative environmental effects). The black cool pigments prepared based on systems previously described in the literature [1] are the following.

(A) Classical Cr doped hematite Fe_2O_3 (trigonal, *R-3c*) solid solution pigment in the optimal composition $\text{Fe}_{1.2}\text{Cr}_{0.8}\text{O}_3$ employed in photocatalysis [15]. This pigment shows tendency to produce brown hues in glazes due to entrance of Zn^{2+} , Mg^{2+} or Al^{3+} from the glazes into pigment lattice [16, 17]; instead it show a good behavior in porcelain stoneware applications. Its high NIR reflectance and the rise in price and toxic characteristics of cobalt-based black pigments has increased the interests in this pigment [1, 16-18]. A commercial pigment supplied by ELCOM SL is used as cool black reference (see Figure 17).

(B) YMnO_3 (hexagonal, $P6_3cm$) hexagonal perovskite. Rare earth distorted perovskite RMnO_3 ($R = \text{Y, La}$) are attracting considerable theoretical and technological interest by virtue of their unusual magnetic and electronic properties ('colossal' magnetoresistance in LaMnO_3) [19] or as heat reflecting blue pigments for energy-saving coatings (exceptionally high NIR reflectance in In doped YMnO_3) [20]. YMnO_3 crystallizes in acentric space group $P6_3cm$ with Mn^{3+} in trigonal-bipyramidal coordination and Y^{3+} 7-fold coordinated; the unit cell contracts 66% with temperature to a $P63/mmc$ form where Y^{3+} shows octahedral coordination [21].

(C) $\text{Sr}_4\text{CuMn}_2\text{O}_9$ (trigonal, $P321$) hexagonal perovskite. The structure and the electric and magnetic properties of disordered hexagonal perovskite-type oxides A_xMO_3 ($A=\text{Sr, M}=\text{Co, Ni}$) have received much attention [22, 23]. The structures of these oxides can be viewed in terms of infinite (MO_3) and A chains, where the (MO_3) chains are made up of face-sharing MO_6 octahedra and trigonal prisms. In the (MO_3) chains, single MO_6 trigonal prisms may alternate with single MO_6 octahedra or with $\text{M}_n\text{O}_{3n+3}$ octahedral oligomers made up of n face-sharing MO_6 octahedra. Crystals of $\text{Sr}_4\text{Mn}_2\text{CuO}_9$ belong to the family of $\text{A}_{1+x}(\text{A}'_x\text{B}_{1-x})\text{O}_3$ ($0 \leq x \leq 1/2$), which is closely related to the hexagonal perovskite 2H structure having a $P321$ space group. The Mn^{4+} ions occupy the octahedral site and Cu^{2+} ions randomly fill the center of the square faces of the trigonal prisms. Mn^{4+} ion can have spin-exchange interactions with adjacent Mn^{4+} ions and also with adjacent Cu^{2+} located at the TP centers. Thus, a number of different local spin arrangements are possible in $\text{Sr}_{4/3}\text{Mn}_{2/3}\text{Cu}_{1/3}\text{O}_3$ disordered hexagonal perovskite-type which has been studied as orange cool pigments doped with Zn^{2+} ($\text{Sr}_4\text{Mn}_2(\text{Cu}_x\text{Zn}_{1-x})\text{O}_9$) [24].

(D) Melilite $\text{Sr}_2(\text{Mg}_{0.5}\text{Mn}_{0.5})\text{Ge}_2\text{O}_7$ (tetragonal, $P-42_1m$). Melilite-type compounds with a general formula $\text{Sr}_2\text{MGe}_2\text{O}_7$ ($M=\text{Mg, Zn, Co, Mn}$) consist of M^{2+} and Ge^{4+} ions which occupy two kinds of tetrahedral sites in an ordered manner in tetrahedral coordination without excess oxygen. The M ions form a square-planar lattice in the ab plane [25]. As the content of Mn in the $\text{Sr}_2(\text{Mg}_{1-x}\text{Mn}_x)\text{Ge}_2\text{O}_{7+\delta}$ solid solutions was increased, the color changed from white to sky blue, deep blue, and finally black body color. $\text{Sr}_2\text{MgGe}_2\text{O}_7$ has the melilite-type structure comprising MgO_4 and GeO_4 tetrahedra. Kim *et al.* [26] found that Mn ion in $\text{Sr}_2(\text{Mg}_{1-x}\text{Mn}_x)\text{Ge}_2\text{O}_{7+\delta}$ solid solutions is mainly trivalent and that the additional oxygen atom infiltrates into the lattice to compensate for the excess positive charge. The

additional oxygen atom occupies an interstitial site, leading to the formation of the rarely Mn^{3+}O_5 trigonal bipyramid and Ge^{4+}O_5 square pyramid. As the driving force for the Mn^{3+}O_5 formation, the tendency for improving the lattice coherency between BO_4 - $\text{B}'\text{O}_4$ and AO_8 layers in the melilite $\text{A}_2\text{BB}'_2\text{O}_7$ is suggested [26].

Precursors, supplied by ALDRICH, with a particle size between 0.3-5 μm were mechanically homogenized in an electric grinder (20000 rpm) during 5 min and the mixture fired at the corresponding temperature and soaking time: 1200°C/3h (pigment A), 1250°C/6h (pigment B), 1000°C/12h (pigment C) and 1250°C/6h (pigment D). In the case of $\text{Sr}_4\text{CuMn}_2\text{O}_9$ hexagonal perovskite (C pigment) a coprecipitation method CO was also carried out in order to check the effect of non-conventional methods. In this CO method, nitrates of the corresponding ions ($\text{Sr}(\text{NO}_3)_2$, $\text{Cu}(\text{NO}_3)_2 \cdot 2\frac{1}{2} \text{H}_2\text{O}$ and $\text{Mn}(\text{NO}_3)_2 \cdot 4\text{H}_2\text{O}$) are solved in water and then ammonia was added drop by drop until gelation occurs. The gel was dried at 110°C and finally fired at 1000°C/6h.

2.2. Samples Characterization

X-Ray Diffraction (XRD) was carried out on a Siemens D5000 diffractometer using Cu K_α radiation (10-70 $^\circ 2\theta$ range, scan rate 0.02 $^\circ 2\theta/\text{s}$, 4 s per step and 40 kV and 20 mA conditions).

$L^*a^*b^*$ and C^*h^* color parameters of glazed samples were measured following the CIE- $L^*a^*b^*$ (Commission Internationale de l'Éclairage) colorimetric method [27] using a X-Rite SP60 spectrometer, with standard lighting D65 and 10° observer. On this method, L^* is a measure of lightness (100=white, 0=black) and a^* and b^* of color parameters ($-a^*$ =green, $+a^*$ =red, $-b^*$ =blue, $+b^*$ =yellow). The values of C^* and h^* and the tolerance ΔE^* based can be estimated from L^* , a^* and b^* parameters by the equations 1-3 respectively:

$$C^* = (a^{*2} + b^{*2})^{1/2} \quad (\text{eq. 1})$$

$$h^* = \arctan (b^*/a^*) \quad (\text{eq. 2})$$

$$\Delta E^* = \sqrt{\Delta L^{*2} + \Delta a^{*2} + \Delta b^{*2}} \quad (\text{eq. 3})$$

ISO 12642-25 (referred to graphic technology to characterize 4-color printing process) considers unacceptable a difference $\Delta E^* > 5$. Instead, the International Standard ISO 10545-16 for ceramic tiles establishes a limit of $\Delta E^* < 0.75$ in part 16, concerning the determination of small color differences between plain

colored ceramic tiles, which are designed to be of uniform and consistent color.

UV-Vis-NIR spectra of fired powder samples and also of the applications of the pigments samples were collected using a Jasco V670 spectrometer through diffuse reflectance technique, which gives data in absorbance using arbitrary units (A) or in reflectance units (R(%)). Band gap energy of semiconductors was calculated by Tauc plot [28] using the UV-Vis-NIR spectra of Kubelka-Munk model [29]. The optical reflectance spectra were scanned in the range of 350 to 2500 nm for optimized pigments. The total solar reflectance R, the solar reflectance in the NIR range R_{NIR} or the solar reflectance in the Vis range are evaluated from UV-Vis-NIR spectra through diffuse reflectance technique as the integral of the measured spectral reflectance and the solar irradiance divided by the integral of the solar irradiance in the range of 350 to 2500 nm for R, 700 to 2500 nm for R_{NIR} or 350-700 nm for R_{VIS} as in the equation 4:

$$R = \frac{\int_{350}^{2500} r(\lambda)i(\lambda)d\lambda}{\int_{350}^{2500} i(\lambda)d\lambda} \quad (\text{eq. 4})$$

Where, $r(\lambda)$ is the spectral reflectance (Wm^{-2}) measured from UV-Vis-NIR spectroscopy and $i(\lambda)$ is the standard solar irradiance ($\text{Wm}^{-2}\text{nm}^{-1}$) according to the American Society for Testing and Materials (ASTM) Standard G173-03.

Microstructure characterization of powders was carried out by Scanning Electron Microscopy (SEM) using a JEOL 7001F electron microscope (following conventional preparation and imaging techniques). The chemical composition and homogeneity of the samples was determined by semi-quantitative elemental analysis with an EDX (Energy Dispersive X-Ray Spectroscopy) analyzer (supplied by Oxford University) attached to the microscope. EDX is a suitable technique for routine quantitative analysis of elements heavier than sodium, present in 10 wt% or greater in the sample and occupying few cubic micrometers of the specimen at least. Trace elements present in <1.0 wt% can be analyzed but with lower precision compared with analyses of elements present in greater concentration [30]

The photoactivity of the samples has been evaluated by the degradation of the azo dye Orange II (OII) in aqueous solutions. The photocatalytic tests were carried out adding a catalyst loading of 0.5 g/l to an OII solution of $0.6 \cdot 10^{-4}$ mol/l, which has been

prepared dissolving an amount of Orange II ($\text{C}_{16}\text{H}_{11}\text{N}_2\text{NaO}_4\text{S}$) in a pH 7.42 phosphate buffer media (NaH_2PO_4 , H_2O 3.31 g and Na_2HPO_4 , $7\text{H}_2\text{O}$ 33.77 g solved in 1 liter of water). The UV irradiation source was a mercury lamp of 125 W emitting in the range 254-365 nm. Before measuring, the suspensions were first stirred in the dark during 15 min to reach sorption/desorption equilibrium. The evolution of reaction was followed taking samples every 15 min. Orange II concentrations in the different sample were determined by means of UV-Vis spectroscopy at 485 nm. The commercial TiO_2 Degussa P25 was used as reference of comparison with the home prepared samples; likewise a CONTROL test without photocatalyst addition is also carried out.

Photocatalytic degradation has been followed according to the Langmuir-Hinshelwood model of heterogeneous catalysis that considers the reaction between two species adsorbed on the catalyst (adsorbates) versus the so-called Eley-Rideal model that postulates the reaction between an adsorbate and an incoming molecule [31]. In the Langmuir-Hinshelwood model at low adsorption and also at low concentration, the degradation turns out to be a pseudo first order kinetics according to the equation 5:

$$\frac{dc}{dt} = Kkc \quad (\text{eq. 5})$$

Where k is the light intensity dependent rate constant, K is the adsorption constant and c is the concentration of degraded compound in the media. Integrating between the initial conditions $t = 0$, $c = c_0$ and at time t:

$$\ln c/c_0 = Kkt \quad (\text{eq. 6})$$

As the light absorption A at 485 nm by the Orange II is directly proportional to its concentration c; the representation of $\ln A/A_0$ against t is a line that passes through the origin and slope Kk. Therefore the photodegradation half-life period $t_{1/2}$ or the time required to degrade to half the substrate content is done by equation 7:

$$t_{1/2} = -\frac{\ln 2}{Kk} \quad (\text{eq.7})$$

2.3. Application of Pigments

The coloring capacity of the pigments was studied in 10 wt% in colorless alkyd paint (Table 1 and Figure 1-2) with a good performance in all cases (L^* decreases and R_{NIR} increases in alkyd matrix (Table 1)), and specially in ceramic applications: 3wt%

Table 1: Black Cool Pigments Based on Systems Previously Described in the Literature (A,B,C and D): Reference Powder of Commercial Carbon Black ($L^*a^*b^*=20.2/0.1/0.1$ (powder) $21.6/0.1/0.1$ (10 wt% in Alkyd Paint), $R_{Vis}/R_{NIR}/R=3/3/3$, $C^*=0.14$, $h=45$ (red)

	(A) $Fe_{1.2}Cr_{0.8}O_3$ 1200/3h	(B) $YMnO_3$ 1250/6h	(C) $Sr_4CuMn_2O_9$ 1000/12h	(D) $Sr_2(Mg_{0.5}Mn_{0.5})Ge_2O_7$ 1250/6h
POWDER				
$L^*a^*b^*$	42.3/-0.3/0.6	27.7/-1.2/-3.5	43.9/7.2/6.3	31.8/-0.1/-8.3
ΔE^*	22.1	3.6	25.5	14.3
C^*	0.7	3.7	9.6	8.3
h (color region)	116.6 (green)	199 (green-blue)	41.2 (red)	269 (blue)
$R_{Vis}/R_{NIR}/R$	4/23/14	3/39/19	7/51/29	5/32/17
E_g (eV)	1.13	1.36	1.38	1.24
10wt% ALKYD PAINT				
$L^*a^*b^*$	39/1.3/0.5	26.2/-2/-4.1	41.2/8.6/6.8	29.6/-0.3/-9.1
$R_{Vis}/R_{NIR}/R$	4/36/21	3/42/23	7/55/30	5/35/19

applications of black cool pigments (A,B,C and D) added in two kind of glazes (double firing glaze at 1000°C and single firing glaze at 1080°C) and 2wt% added to porcelain stoneware powder. The technical characteristics of the glazes are described below.

Cool pigments should present high values of R and R_{NIR} along with high stability and coloring capacity in its applications, showing high chroma C^* (except for black hues which tends to zero) and lightness L^* should be enclosed within the range of Munsell's high chromaticity for the different hues: e.g. high for yellow (80-90), cyan (75-85) and green (70-80), middle for magenta (50-60) and red (45-55) and low for blue (25-35) and black (35-0) hues [32]. Authors have associated the high reflectance or SRI (Solar

Reflectance Index) with the lightness L^* or Y factor. For instance, L.M. Schabbacha *et al.* analyzed the thermal and optical properties related to solar reflectance index in pigmented glazed ceramic roof tiles in Brazil [33]: the results show that most of the colored glazed tiles did not meet the 2013 LEED requirement, that is, $SRI \geq 39$ for roof tiles with a steep slope. A polynomial relationship between the Y factor (or L^*) and the SRI (or R) was found (R^2 value > 0.95), and thus the tile colors would probably not qualify for SRI certification.

3. RESULTS AND DISCUSSION

3.1. Black Cool Powder Pigments (A,B,C, D)

Figure 4 shows the powders image and the corresponding XRD pattern of the black cool pigments

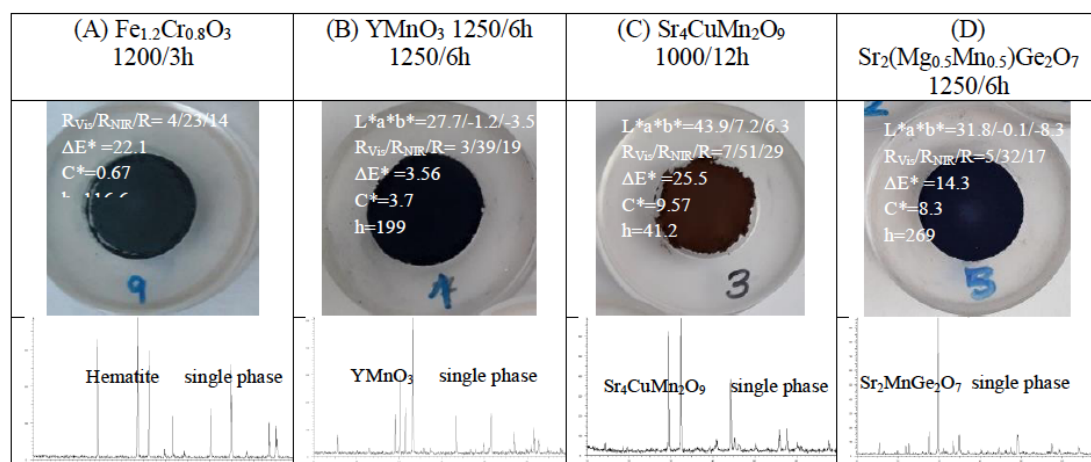


Figure 4: Black cool pigments based on systems previously described in the literature (A,B,C,D) [17, 19, 24, 26]: reference commercial carbon black ($L^*a^*b^*=20.2/0.1/0.1$, $R_{Vis}/R_{NIR}/R=3/3/3$, $C^*=0.14$, $h=45$ (red)).

powders based on systems previously described in the literature (A,B,C,D) and Table 1 summarizes its color characterization, reflectance and bandgap measurements using as reference a commercial carbon black ($L^*a^*b^*=20,2/0,1/0,1$, $R_{\text{Vis}}/R_{\text{NIR}}/R=3/3/3$, $C^*=0,14$, $h=45$ (red)).

The XRD patterns show the crystallization of the corresponding single crystalline phase in each pigment: hematite Fe_2O_3 (trigonal, $R-3c$) in (A) $\text{Fe}_{1.2}\text{Cr}_{0.8}\text{O}_3$, YMnO_3 distorted perovskite (hexagonal, $P6_3cm$) in (B), $\text{Sr}_4\text{CuMn}_2\text{O}_9$ hexagonal perovskite (trigonal, $P321$) in (C), and melilite $\text{Sr}_2\text{MgGe}_2\text{O}_7$ (tetragonal, $P-42_1m$) in (D) $\text{Sr}_2(\text{Mg}_{0.5}\text{Mn}_{0.5})\text{Ge}_2\text{O}_7$ pigment.

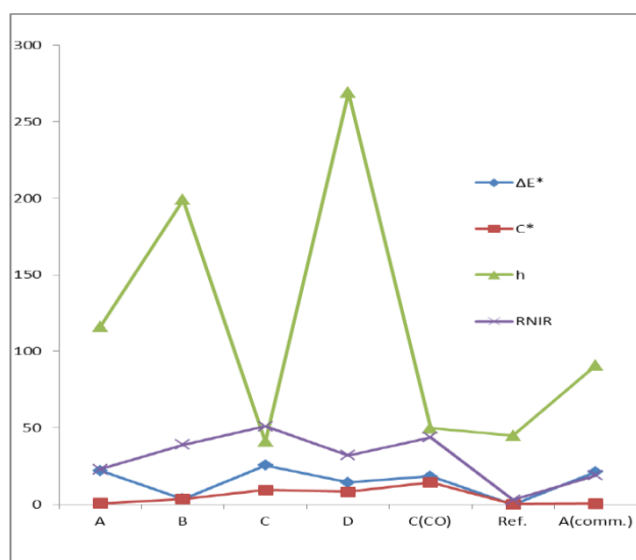


Figure 5: Black cool pigments based on systems previously described in the literature [17, 19, 24, 26]: A,B,C,D, C(CO) prepared by CO method, A(comm.): commercial Cr-hematite pigment, Ref.: carbon black commercial reference.

The $L^*a^*b^*$ color results in Table 1 represented in Figure 5 show that lightness L^* is enclosed within the above described range of Munsell's high chromaticity for (A) $\text{Fe}_{1.2}\text{Cr}_{0.8}\text{O}_3$ ($L^*=27.7$) and (D) $\text{Sr}_2(\text{MgMn})\text{Ge}_2\text{O}_7$ ($L^*=31.8$) but (B) YMnO_3 and (C) $\text{Sr}_4\text{CuMn}_2\text{O}_9$ pigments are not enclosed showing L^* around 43. On the other hand (B) YMnO_3 is the nearest black color to the carbon black reference with $\Delta E^*=3.7$, followed by (D) $\text{Sr}_2(\text{MgMn})\text{Ge}_2\text{O}_7$ ($\Delta E^*=14.3$), (A) $\text{Fe}_{1.2}\text{Cr}_{0.8}\text{O}_3$ ($\Delta E^*=22.1$) and (C) $\text{Sr}_4\text{CuMn}_2\text{O}_9$ ($\Delta E^*=25.5$). The nearest chroma C^* parameter to the carbon black reference is for A ($C^*=0.7$), the sample B ($C^*=3.7$) show a low relative value also, the samples D and C with higher values tend to blue ($b^*=-8.3$) in the case of germanate D and to green-yellow for C sample. Finally, only the sample C shows a hue similar to reference

($h=41.2$ (red region)), the hue of A and B tend to green region and D to blue. The Cr-hematite commercial black pigment supplied by Elcom S.L. shows $\Delta E^*=21.3$ and $C^*=0.6$ very close to its homologous composition A, however the hue $h=91$ (orange-green) is different (Figure 17).

The reflectance data in Table 1 and Figure 4 show that R_{NIR} decreases in the sequence C (51%), B(39%), D (32%) and finally A(23%). Therefore the pigment (C) $\text{Sr}_4\text{CuMn}_2\text{O}_9$ shows the nearest hue h to the reference carbon black but with very high NIR reflectance. However the pigment (B) YMnO_3 shows the lower color tolerance ΔE^* from the reference and the (A) $\text{Fe}_{1.2}\text{Cr}_{0.8}\text{O}_3$ pigment shows the minimum L^* and chroma of the serie (best black chroma).

Figure 6 shows the UV-Vis-NIR reflectance spectra of black cool pigments of the series A,B,C,D and the reference, showing the sequence in the R_{NIR} above described. The spectra give interesting data about the valence of the ions, their coordination and the mechanism of color in the system [1].

For (A) $\text{Fe}_{1.2}\text{Cr}_{0.8}\text{O}_3$ pigment the diffuse reflectance spectrum of $\text{Fe}_{1.2}\text{Cr}_{0.8}\text{O}_3$ is integrated by broad bands at 450 nm, 680 nm and 940 nm (minimums of reflectance in Figure 6A). Usually this pigment is considered a substitutional solid solution with a corundum-type crystalline network. The Fe^{3+} and Cr^{3+} cations occupy two-thirds of the octahedral vacancies in the compact hexagonal network formed by the oxygen anions, and are randomly distributed according to their proportion in the mixture.

Figure 7 shows the UV-Vis-NIR diffuse reflectance spectra of the (A) $\text{Fe}_{1.2}\text{Cr}_{0.8}\text{O}_3$ black cool pigment and its precursors: hematite (Fe_2O_3) and eskolaite (Cr_2O_3). Cr^{3+} (d^3) in octahedral coordination in eskolaite lattice shows a cation-anion charge transfer band at 250 nm (not shown) and two intense, parity-forbidden and spin-allowed transitions: ${}^4A_{2g}(4F) \rightarrow {}^4T_{2g}(4F)$ at 600 nm and ${}^4A_{2g}(4F) \rightarrow {}^4T_{1g}(4F)$ at 420 nm, and furthermore tiny bands at 700 and 920 nm associated to doubly forbidden transition to ${}^2T_{1g}(2G)$ and ${}^2E_g(2G)$ respectively [34]. On the other hand, Fe^{3+} (d^5) in octahedral coordination in hematite lattice shows an intense charge transfer band at 290-310 nm (not shown), spin forbidden transitions from the ground state ${}^6A_1(6S)$ to 4E and 4A (4G) at 400 nm and Fe^{3+} spin forbidden transitions from the ground state 6A_1 to

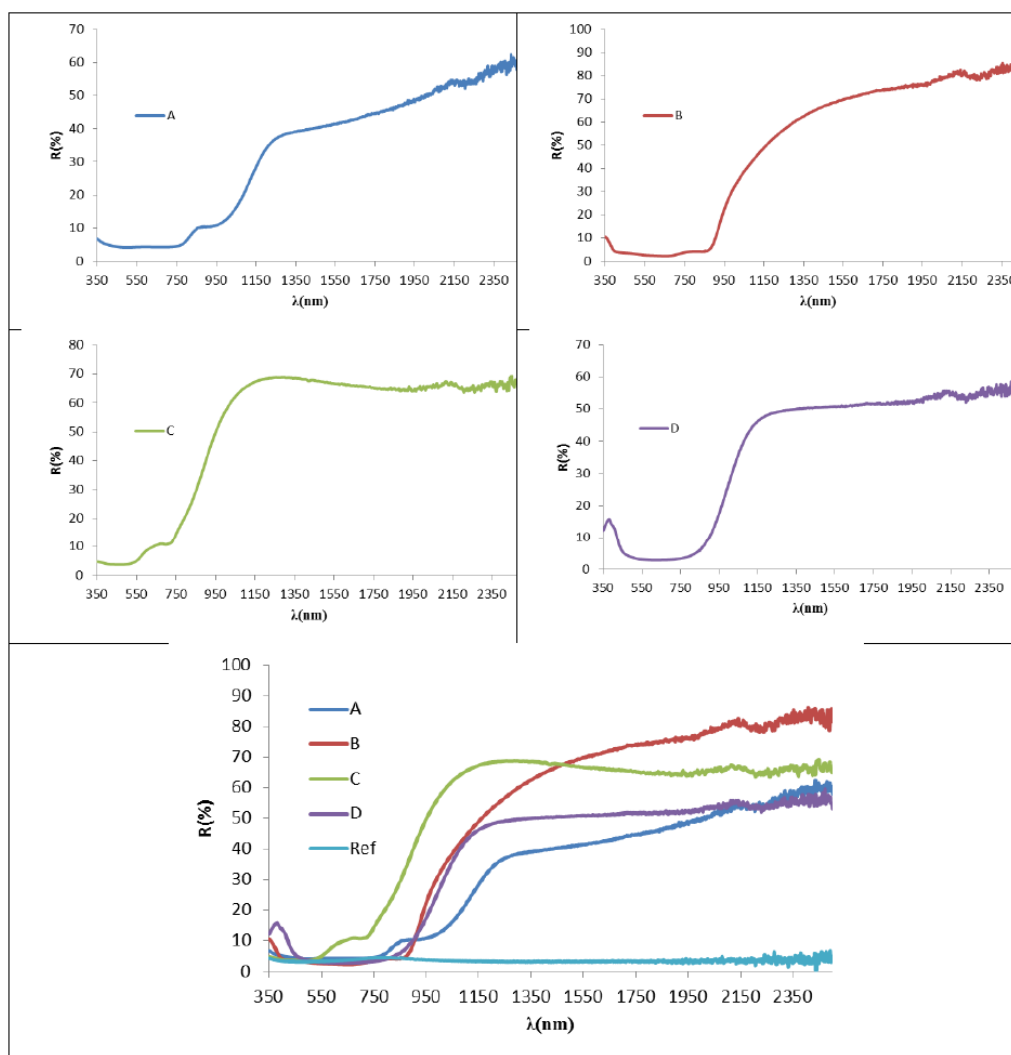


Figure 6: UV-Vis-NIR reflectance spectra of black cool pigments based on systems previously described in the literature [17, 19, 24, 26]: **A,B,C,D** and the series compared with carbon black reference.

the excited states 4T_2 and 4T_1 , whose configuration is $(t_{2g})^4(e_g)^1$ at 650 and 900 nm respectively [35].

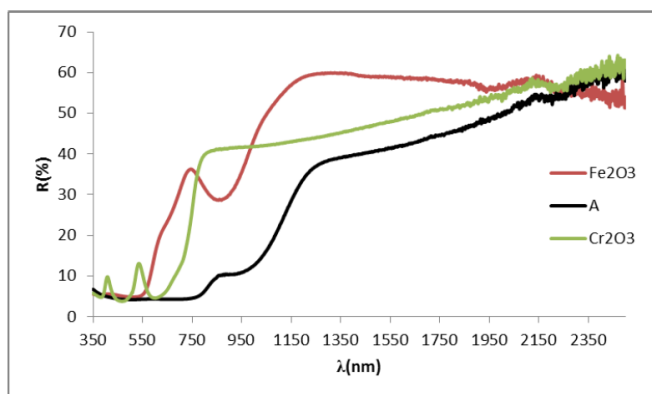


Figure 7: UV-Vis-NIR diffuse reflectance spectra of (A) $\text{Fe}_{1.2}\text{Cr}_{0.8}\text{O}_3$ black cool pigment and its precursors hematite (Fe_2O_3) and eskolaite (Cr_2O_3).

The bands for the (A) $\text{Fe}_{1.2}\text{Cr}_{0.8}\text{O}_3$ pigment in Figure 7 are consistent with the solid solution eskolaite-hematite by overlapping of Cr^{3+} (d^3) and Fe^{3+} (d^5) absorptions in octahedral environments: the band observed at 450 nm results from the overlapping of Cr^{3+} (${}^4A_{2g}(4F) \rightarrow {}^4T_{1g}(4F)$) and Fe^{3+} (${}^6A_1(6S) \rightarrow {}^4E$ and ${}^4A(4G)$), and the detected at 680 nm from Cr^{3+} (${}^4A_{2g}(4F) \rightarrow {}^4T_{2g}(4F)$) and Fe^{3+} (6A_1 to the excited states 4T_2), finally the band at 940 nm is the result of the overlapping of Cr^{3+} (${}^4A_{2g}(4F) \rightarrow {}^2E_g(2G)$) and Fe^{3+} (6A_1 to the excited states 4T_1). Therefore a crystal field mechanism (CFM) of the chromophore ions Cr^{3+} (d^3) and Fe^{3+} (d^5) in corundum structure is associated to this pigment in agreement with literature [13, 14].

For (B) YMnO_3 pigment, the diffuse reflectance spectrum of YMnO_3 is integrated by broad bands at 420 nm, 640 nm and 860 nm (Figure 6B): a crystal field

mechanism (CFM) explain the black color of YMnO_3 associated to the D_{3h} trigonal bipyramid allowed transition between the valence-band maximum, composed of Mn $3d_{(x^2-y^2,xy)}$ states strongly hybridized with O $2p_{(x,y)}$ states, and the narrow Mn $3d_z^2$ -based conduction-band minimum of $\text{Mn}^{3+}(3d^4)$ ion with a double band at 640 and 860 nm and the charge transfer band $\text{O}_{2p(x,y)} \rightarrow \text{Mn } 3d_z^2$ at 420 nm [20].

In the case of (C) $\text{Sr}_4\text{CuMn}_2\text{O}_9$ pigment, the minimum of the broad reflectance bands is detected at 400, 540 and 730 nm (Figure 6C). $\text{Mn}^{4+}(d^3)$ in octahedral coordination shows in agreement with Tanabe Sugano diagrams [36] a parity-forbidden and spin-allowed transitions ${}^4A_{2g}(4F) \rightarrow {}^4T_{2g}(4F)$ and ${}^4A_{2g}(4F) \rightarrow {}^4T_{1g}(4F)$ compatible with the observed bands at 540 and 400 nm respectively in C pigment; furthermore tiny bands associated to doubly forbidden transition to ${}^2T_{1g}(2G)$ (compatible with the position of band at 730 nm but not with its high intensity) and to ${}^2E_g(2G)$ (not detected) respectively. On the other hand Cu^{2+} shows an outer electron configuration $3d^9$ and may be formally be treated as a $3d^1$ within the electron-hole formalism. In this case Cu^{2+} ions randomly fill the center of the square faces of the trigonal prisms showing square-plane coordination which in the Egyptian Blue pigment [37,38] shows weak d–d transitions of copper (despite symmetry very close to D_{4h} of copper coordination) due to vibronic coupling: with bands at 800 nm associated with (${}^2B_{1g} \rightarrow {}^2B_{2g}$), at 650 nm with (${}^2B_{1g} \rightarrow {}^2E_g$) and at 540 nm with (${}^2B_{1g} \rightarrow {}^2A_{1g}$). Therefore the overlapping absorption bands described for $\text{Mn}^{4+}(d^3)$ in octahedral coordination and Cu^{2+} ions in square-plane coordination can explain the positions of the bands reflectance spectra of (C) $\text{Sr}_4\text{CuMn}_2\text{O}_9$ pigment in Figure 6C, however it is not able to justify its anomalously high optical density, therefore spin-exchange interactions of Mn^{4+} ions with adjacent Mn^{4+}

ions and also with adjacent Cu^{2+} located at the TP centers should be considered for explain the high intensity of absorption in the visible region by a Paired spin exchange transitions (PET) [1].

For (D) Melilite $\text{Sr}_2(\text{Mg}_{0.5}\text{Mn}_{0.5})\text{Ge}_2\text{O}_7$ pigment, only a broad band extended from 500 to 800 nm is detected (Figure 6D). Considering a simple replacement of Mg^{2+} by $\text{Mn}^{2+}(d^5)$ in tetrahedral environment; parity-forbidden and spin-allowed transitions ${}^4A_{2g}(4F) \rightarrow {}^4T_{2g}(4F)$ at around 600 nm and ${}^4A_{2g}(4F) \rightarrow {}^4T_{1g}(4F)$ at about 400 nm, and also tiny bands at 700-1000 nm associated to doubly forbidden transition to ${}^2T_{1g}(2G)$ and ${}^2E_g(2G)$ respectively, are predicted in agreement with Tanabe Sugano diagrams, that are not compatible with Figure 3. Mg^{2+} (Shannon-Prewit radius 0.71 Å in tetrahedral coordination) can be replaced by the similarly sized $\text{Mn}^{3+}(d^4)$ ion (Shannon-Prewit radius 0.72 Å in fivefold coordination and in octahedral low spin,; there are not data for tetrahedral environment [39]), but for the preservation of lattice electroneutrality, vacancies of Mg^{2+} (or Mn^{3+}) or addition of oxygen ions infiltrated in the lattice should be considered. According to Tanabe Sugano diagram $\text{Mn}^{3+}(d^4)$ in tetrahedral coordination shows a band due to ${}^5T_{2g} \rightarrow {}^5E_{2g}$ transition compatible with Figure 3D [36]. As above discussed, Kim *et al.* [26] found that Mn ion is mainly trivalent, showing $\text{Mn}^{(3+)}\text{O}_5$ trigonal bipyramid (and $\text{Ge}^{(4+)}\text{O}_5$ square pyramid) and additional oxygen atoms occupies an interstitial site, leading to the formation of $\text{Sr}_2(\text{Mg}_{1-x}\text{Mn}_x)\text{Ge}_2\text{O}_{7+\delta}$ solid solutions. Probably a intervalence charge transfer mechanism $\text{Mn}^{3+} - \text{Mn}^{2+}$ is involved to produce the color (IVCTM) [1].

Figure 8 shows the Kubelka Munk absorption spectra of representative pigments. An ideal black NIR reflective pigment would show $R_{\text{vis}}=0$ (from Vis range 380–750 nm) and $R_{\text{NIR}}=100$ (from NIR range 700–2500 nm); therefore its inflection point of the diffuse

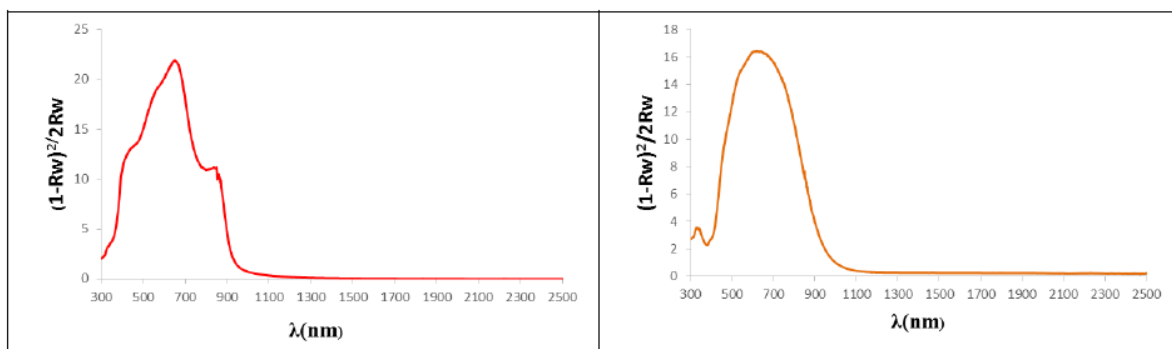


Figure 8: Kubelka Munk absorption spectra of (B) YMnO_3 and (D) Melilite $\text{Sr}_2(\text{Mg}_{0.5}\text{Mn}_{0.5})\text{Ge}_2\text{O}_7$ pigments.

reflectance spectrum should be at ~ 750 nm (1.65 eV). E_g data measured from Kubelka Munk absorption spectra using the Tauc *et al.* method [28] for the black pigments in Table 1 are into the range 1.38 eV (900 nm) for (C) $\text{Sr}_4\text{CuMn}_2\text{O}_9$ (the nearest to ideal bandgap), 1.36 eV (910 nm) for (B) YMnO_3 , 1.24 eV (1000 nm) for (D) $\text{Sr}_2(\text{MgMn})\text{Ge}_2\text{O}_7$ and 1.13 eV (1100 nm) for (A) $\text{Fe}_{1.2}\text{Cr}_{0.8}\text{O}_3$; the same progression that for R_{NIR} values of 51, 39, 32 and 23% respectively.

Figure 9 shows SEM micrographs of black cool pigments A, B, C, D. (A) $\text{Fe}_{1.2}\text{Cr}_{0.8}\text{O}_3$ pigment shows the best faceted crystallization of rhombohedral crystals with a particle size of 2-6 μm . (B) YMnO_3 pigment

shows fine particles of 1 μm which form aggregates of 2-6 μm of size. (C) $\text{Sr}_4\text{CuMn}_2\text{O}_9$ and (D) $\text{Sr}_2(\text{Mg}_{0.5}\text{Mn}_{0.5})\text{Ge}_2\text{O}_7$ pigments show similar and very fine (0.5-1 μm) particles. The compositional analysis by EDX mapping of the samples shows a homogeneous distribution of the ions in the particles (Figure 10).

3.2. Application in Glazes of the Black Cool Pigments (A,B,C,D)

Table 2 shows the SEM micrograph and chemical composition (obtained by EDX analysis) of the used glazes and porcelain stoneware powders and also in alkyd paint (based on alkyd resins or organic polyesters such as the derived from phthalic anhydride

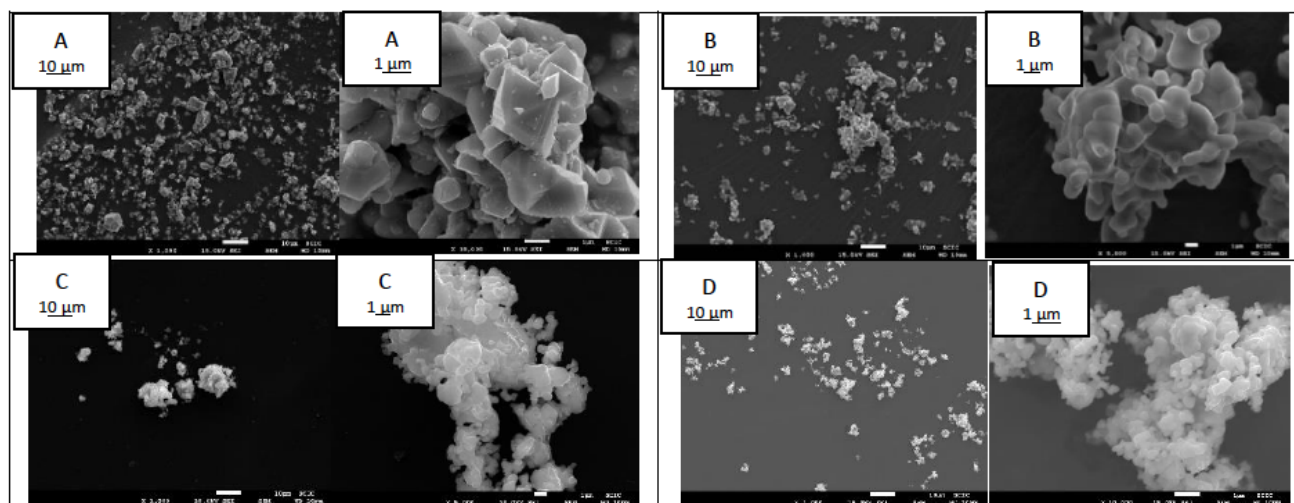


Figure 9: SEM micrographs of black cool pigments A,B,C, D.

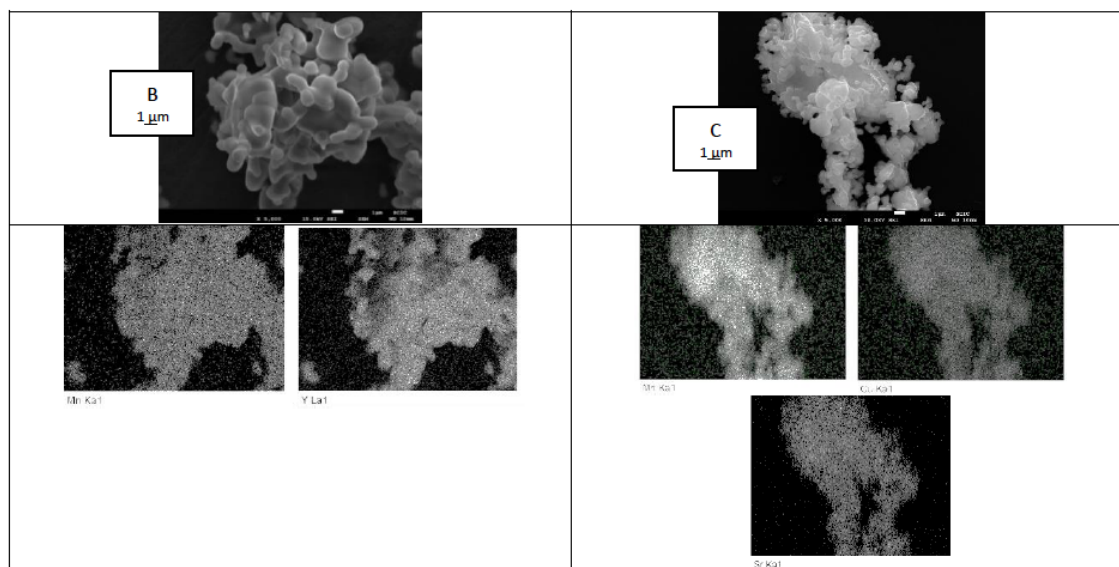

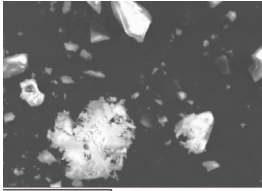
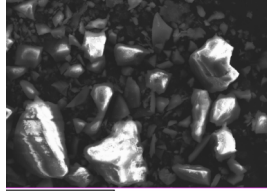


Figure 10: Analysis by EDX mapping of (B) YMnO_3 and (C) $\text{Sr}_4\text{CuMn}_2\text{O}_9$ powder pigments.

Table 2: SEM Micrograph and Chemical Composition (Obtained by EDX Analysis in wt%) of the Used Glazes and Porcelain Stoneware Powder

	Double Firing (1000°C)	Single Firing (1080°C)	Porcelain Stoneware (1190°C)
oxide			
SiO ₂	75	65	67
Na ₂ O	5	2	-
K ₂ O	2	4	3
CaO	2	11	12,5
MgO	-	2	1,5
ZnO	-	7,5	6,5
Al ₂ O ₃	10	8,5	9
PbO	6	-	-

and glycerol). Figure 11 shows the thermal firing cycle used with employed glazes and porcelain stoneware.

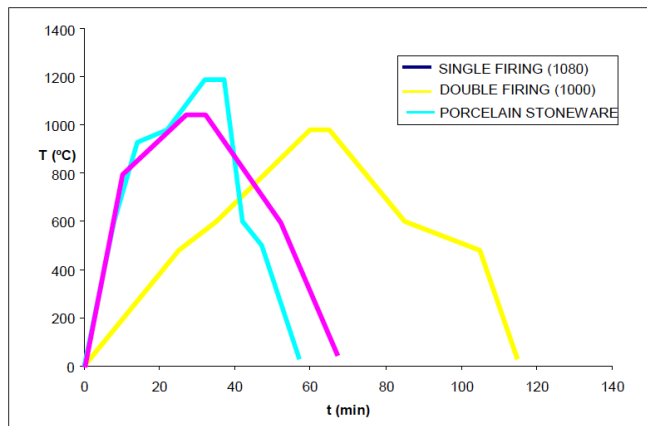


Figure 11: Thermal firing cycle used with glazes and Porcelain Stoneware employed.

Table 3 and Figure 12 summarize the results of the characterization of the 3wt% applications of black cool pigments (A,B,C,D) added in two kind of glazes (double firing glaze at 1000°C and single firing glaze at 1080°C) and 2wt% added to porcelain stoneware powder (manually homogenized in a mortar and pressed into pellets at 150 kg/cm² and fired at 1200°C), using as black reference the powder of commercial carbon black (L*a*b*=20.2/0.1/0.1, R_{vis}/R_{NIR}/R= 3/3/3, C*=0.14, h=45 (red).

(A) Fe_{1.2}Cr_{0.8}O₃ pigment shows a black and stable performance in the low temperature glaze (ZnO free, Table 2, Figure 12); however, it is brown in the high temperature glaze (with ZnO, Table 2) associated to the reaction and crystallization of brown Zn(Fe,Cr,Al)₂O₄ spinels as it is well known in the literature [16], furthermore in 2wt% added to porcelain stoneware powder, the pigment shows a stable black behavior (L*a*b*=40.9/3.3/5) in agreement with literature [1,16,17]. The reflectance R_{NIR} is relatively high in the black low temperature glaze (17%) and show high values in the brown high temperature glaze (43%) and especially in the black porcelain stoneware pellets (49%).

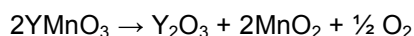
Figure 13 compares the UV-Vis-NIR reflectance spectra of the black (A) Fe_{1.2}Cr_{0.8}O₃ powder and the brown 3wt% double firing glazed sample. Absorption bands (reflectance minimums) are detected in glazed sample at 500, 670 nm in the visible range that have its corresponding bands in the powder spectrum, but the absorption intensity decreases (reflectance increases) for the 670 nm and the black shade is lost and sample appears brown. Likewise a NIR band at 860 is detected that shifts to low wavelength respect the powder (940 nm) and an additional intense NIR band at 1150 nm is detected in this glazed sample but also in the black single firing glazed sample and in the black porcelain

Table 3: Applications of Black Cool Pigments (A,B,C and D) 3% Added in the Indicated Glazes: Reference Powder of Commercial Carbon Black ($L^*a^*b^*=20.2/0.1/0.1$, $R_{vis}/R_{NIR}/R= 3/3/3$, $C^*=0.14$, $h=45$ (red))

	(A) $Fe_{1.2}Cr_{0.8}O_3$ 1200/3h	(B) $YMnO_3$ 1250/6h	(C) $Sr_4CuMn_2O_9$ 1000/12h	(D) $Sr_2(Mg_{0.5}Mn_{0.5})Ge_2O_7$ 1250/6h
3 wt% Double Firing (1000°C)				
$L^*a^*b^*$	34.1/2.6/-3.7	31.9/1.6/1.1	57.9/2.8/0.2	49.6/12.8/13.7
ΔE^*	14.6	11.9	37.8	35
C^*	4.5	2.5	2.8	18.7
h (color region)	125.1 (orange)	50.0 (red)	184.0 (green-blue)	47.0 (red)
$R_{vis}/R_{NIR}/R$	4/17/10	7/31/18	25/41/33	25/68/44
E_g (eV)	1.51	1.36	1.00	1.51
3 wt% Single Firing (1080°C)				
$L^*a^*b^*$	34.1/11.6/4.0	59.3/2.4/1.4	55.2/3.4/3.7	74.8/4.8/1.3 colorless
ΔE^*	18.5	39.2	35.3	54.0
C^*	12.3	2.8	5.0	5.0
h (color region)	19.0 (violet)	30.3 (red)	47.4 (red)	15.2 (violet)
$R_{vis}/R_{NIR}/R$	6/43/24	28/53/39	21/37/29	56/73/64
E_g (eV)	1.43	1.36	1.08	1.55
2 wt% Porcelain Ston (1200°C)				
$L^*a^*b^*$	40.9/3.3/5	colorless	colorless	colorless
ΔE^*	21.2			
C^*	4.8			
h (color region)	46.7 (red)			
$R_{vis}/R_{NIR}/R$	8/49/28			
E_g (eV)	1.43			

stoneware sample (Figure 12) but with lower intensity in this case allowing an higher NIR reflectance.

(B) $YMnO_3$ pigment shows a black and stable performance in the low temperature glaze (ZnO free) but some pin hole, probably associated to the decomposition of the compound to colorless Mn^{2+} that dissolves in the glaze releasing oxygen is detected (Figure 12). Considering oxides:



In effect, manganese with III and IV valence has been traditionally employed (usually in the form of manganese dioxide) as the sometimes colloquially known as “glassmakers’ soap” as key ingredient in the making of reasonably colorless glass. The use of this compound as decolorizer in glassmaking has been

known since at least 1290 associated with its oxidizing action on Fe^{2+} (that induces a greenish color to the glassy mass) to the colorless Fe^{3+} , reducing the Mn (IV) or Mn (III) to the colorless Mn^{2+} [40,41]. In the most aggressive conditions of single firing glaze at 1080°C the decomposition rate increases and a profuse pin hole with loss of black shade is observed (Figure 12). In the case of porcelain stoneware at 1200°C, the decomposition is complete and the sample becomes colorless.

Figure 14 shows a comparison of UV-Vis-NIR reflectance spectra of (B) $YMnO_3$ pigment and its 3 wt% application in the single firing glaze (1000°C). The two spectra are very similar indicating the stabilization of the chromophore agents and then the $YMnO_3$ crystalline phase in the glassy matrix. Only a shoulder at 1200 nm appear in glazed sample that decreases

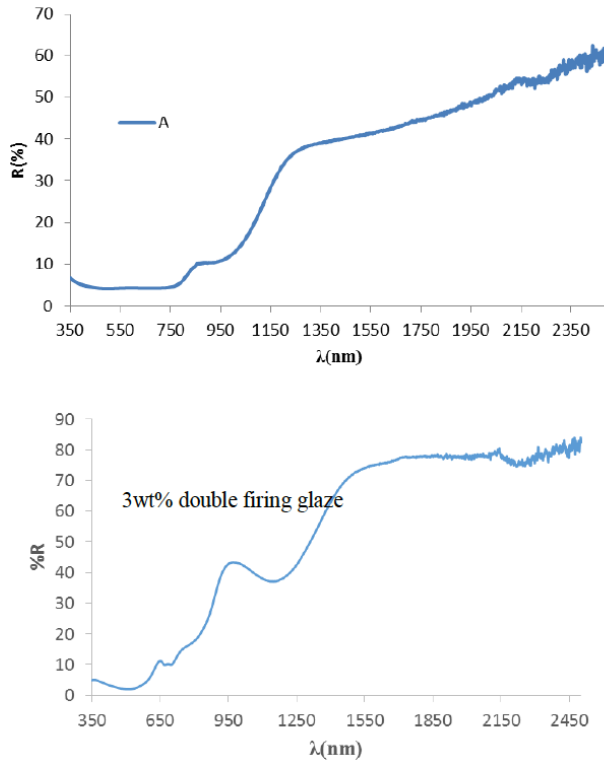


Figure 13: Comparison of UV-Vis-NIR reflectance spectra of (A) Fe_{1.2}Cr_{0.8}O₃ pigment and its 3 wt% application in the double firing glaze (1000°C).

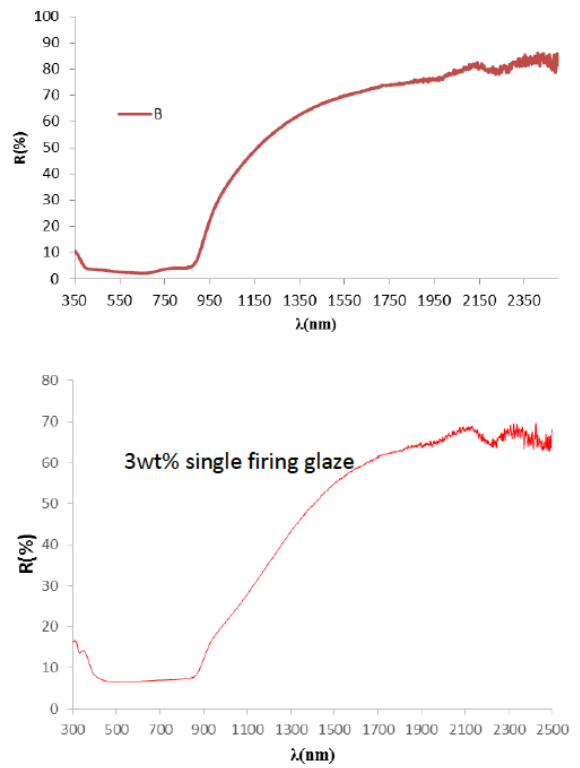


Figure 14: Comparison of UV-Vis-NIR reflectance spectra of (B) YMnO₃ pigment and its 3 wt% application in the single firing glaze (1000°C).

the reflectance in the 1000-1500 nm range, involving a slight decrease in R_{NIR} (39% for powder and 31% for glazed sample) which can be associated to the partial dissolution of Mn²⁺ in the glassy matrix and the microbubbles of oxygen released and trapped into glass.

(C) Sr₄CuMn₂O₉ shows a similar behavior to (B) YMnO₃ pigment, associated with the reduction of Mn⁴⁺ in this case, however the decomposition is less strong in the single firing glaze which presents pin holes but it maintains the black shade (Figure 12).

Figure 15 compares the UV-Vis-NIR reflectance spectra of (C) Sr₄CuMn₂O₉ pigment and its 3wt% application in the single firing glaze (1000°C). Bands at 480 and 740 nm are detected in the glazed sample: the absorption band at 400 nm in powder sample is not detected in glazed sample and, as in the B pigment, a shoulder at 1200 nm appear in glazed sample that decreases the reflectance in the 1000-1500 nm range, involving a slight decrease in R_{NIR} (51% for powder and 41% for single firing glazed and 37% in double firing glazed samples respectively) that can be associated with the partial dissolution of Mn²⁺ in the glassy matrix and the microbubbles of oxygen released and trapped into glass. The decrease of Mn⁴⁺ in the system

(reduced to Mn²⁺ incorporated to glassy matrix) can be associated to the loss of absorption at 400 nm.

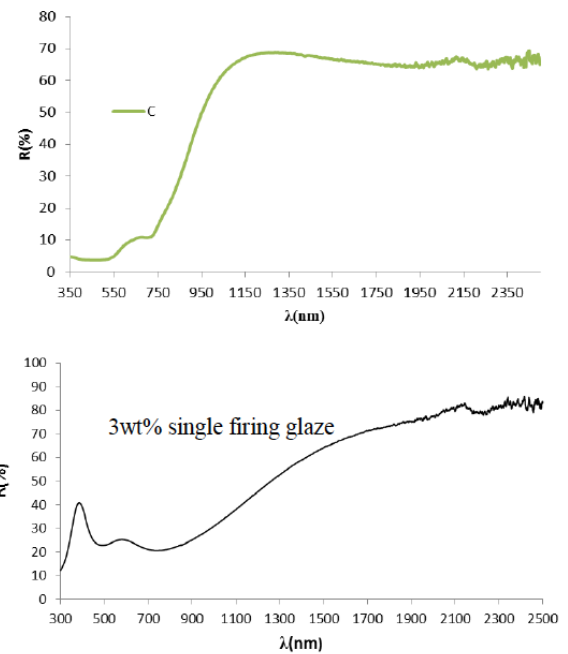


Figure 15: Comparison of UV-Vis-NIR reflectance spectra of (C) Sr₄CuMn₂O₉ pigment and its 3 wt% application in the single firing glaze (1000°C).

(D) $\text{Sr}_2(\text{Mg}_{0.5}\text{Mn}_{0.5})\text{Ge}_2\text{O}_7$ glazed application exhibits unstable behavior similar to B and C pigment, associated to reduction of Mn^{3+} in this case, but the decomposition is strong in both glazes and although the pin hole is moderate, the double firing glazed sample is brown and the single firing one is colorless like the porcelain stoneware sample (not shown) (Figure 12).

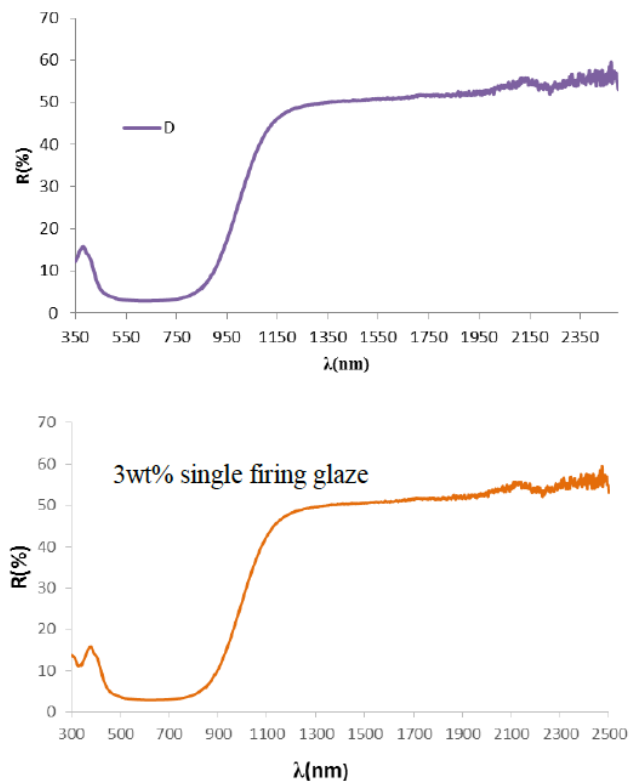


Figure 16: Comparison of UV-Vis-NIR reflectance spectra of (D) $\text{Sr}_2(\text{Mg}_{0.5}\text{Mn}_{0.5})\text{Ge}_2\text{O}_7$ pigment and its 3 wt% application in the single firing glaze (1000°C).

Figure 16 shows the comparison of UV-Vis-NIR reflectance spectra of (D) $\text{Sr}_2(\text{Mg}_{0.5}\text{Mn}_{0.5})\text{Ge}_2\text{O}_7$ pigment and its 3wt% application in the single firing glaze (1000°C). The broad band extended from 500 to 800 nm detected for powder reflectance associated to its black performance disappears in glazed sample which shows absorbance at 300 nm (associated to the a charge transfer from oxygen ions to metals), and an intense band centered at 490 nm that increases reflectance in the 500-1000 nm range, involving a brown color compatible with $\text{Mn}^{3+}(\text{d}^4)$ in tetrahedral coordination in agreement with Tanabe Sugano diagrams [33], indicating a different chromophore scenario. Therefore the melilite with showing Mn^{3+}O_5 trigonal bipyramid and possible intervalence charge transfer $\text{Mn}^{3+} - \text{Mn}^{2+}$ is not stabilized and simply

$\text{Mn}^{3+}(\text{d}^4)$ dissolved in the glassy matrix is responsible of the brown color.

Indeed, for ceramic applications (A) $\text{Fe}_{1.2}\text{Cr}_{0.8}\text{O}_3$ pigment shows good behavior in free ZnO glazes and also in porcelain stoneware, (B) YMnO_3 and (C) $\text{Sr}_4\text{CuMn}_2\text{O}_9$ black pigments can be compatible with low temperature glazes, and finally (D) $\text{Sr}_2(\text{Mg}_{0.5}\text{Mn}_{0.5})\text{Ge}_2\text{O}_7$ pigment loses the black color even in the low temperature glazes, producing brown color.

3.3. Synthesis by Coprecipitation Method

In order to analyses the possible effect of stabilization of the pigment against the glazes, the (C) $\text{Sr}_4\text{CuMn}_2\text{O}_9$ that shows the nearest hue h to the reference carbon black and the maximum NIR reflectance of the series (with the nearest bandgap to an ideal NIR reflective black pigment), has been prepared by ammonia coprecipitation method.

Figure 17 shows the commercial Cr-hematite and a comparison between $\text{Sr}_4\text{CuMn}_2\text{O}_9$ pigments prepared by CE (fired at 1000°C/12h) and CO ((fired at 1000°C/6h. Both samples show $\text{Sr}_4\text{CuMn}_2\text{O}_9$ as single phase detected by XRD. CO sample fired at only 6 h at 1000°C shows better color characteristics than CE pigment fired 12 h at 1000°C: the lightness L^* is lower for CO sample like the tolerance ΔE^* respect carbon black reference (18.4 versus 25.5 for CE sample). However the chroma C^* and hue h^* are higher for CO sample indicating a more brownish shade, its band gap is lower than in CE sample (1.35 eV versus 1.38 eV for CE pigment); in agreement, the R_{NIR} value is also lower (44% versus 51% for CE sample). The 3wt% application in single firing glaze produce a dramatically decomposition of the CO sample with a very profuse pin hole and blueish ($b^*=-4.6$) indicating a lower stability on glazes than CE sample.

Figure 18 shows the comparison of SEM images and EDX mapping between $\text{Sr}_4\text{CuMn}_2\text{O}_9$ pigments prepared by CE (1000°C/12h) and CO (1000°C/6h) methods. Both samples show a homogeneous distribution of ions in the aggregates. CE sample shows particles of 0.5-1 μm forming aggregates of 1-7 μm and CO presents finer particles of 0.5 μm forming aggregates of 2-8 μm . The fine particles in the CO sample react with the glaze and decompose rapidly producing the profuse pin hole observed in the glazed sample.

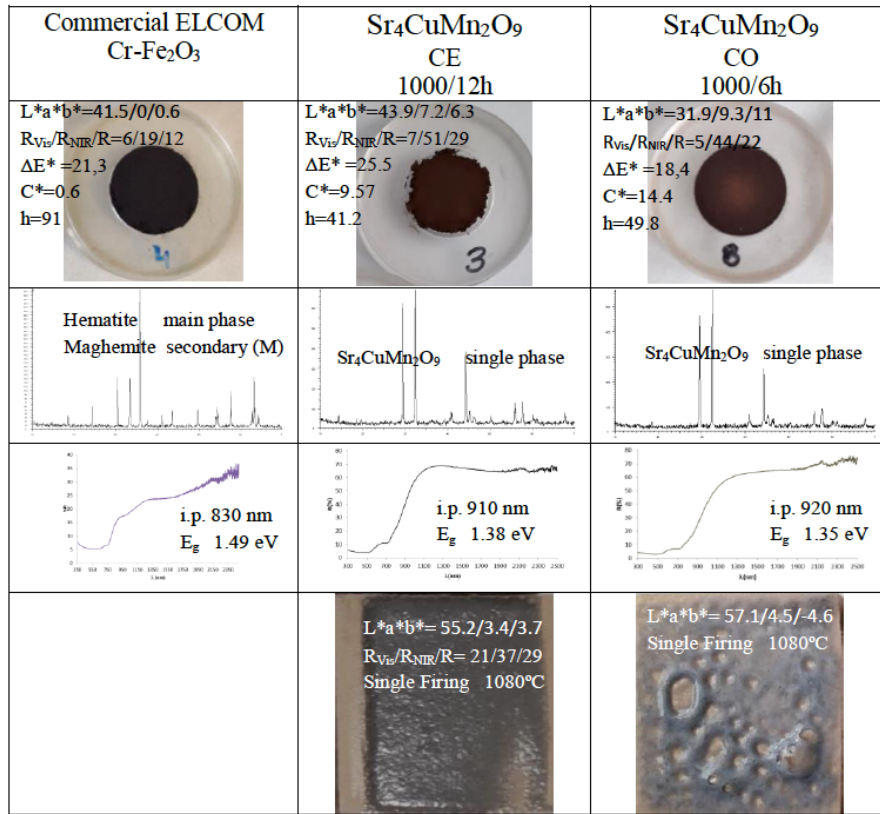


Figure 17: Commercial Cr-hematite and Sr₄CuMn₂O₉ pigment prepared by CE and CO methods.

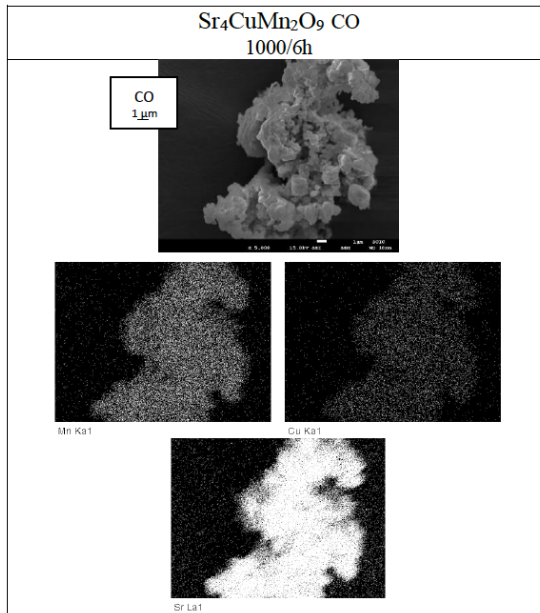


Figure 18: Comparison of SEM and EDX mapping between Sr₄CuMn₂O₉ pigments prepared by CO method (fired at 1000°C/6h)

3.4. Photocatalytic Activity on Orange II Substrate

Table 4 shows the photodegradation parameters ($t_{1/2}$ and the regression coefficient of the corresponding line from equation 6) of Orange II test carried out with

pigment series. Figure 19 presents the respective photodegradation curves: P25 is the usual commercial reference of TiO₂ photocatalyst nanopowder supplied by Degussa [42], CONTROL is the obtained photodegradation carried out without powder addition

Table 4: Photodegradation Parameters of Orange II Test with Powders: P25 (Degussa Reference), CONTROL (Carried out Without Powder), A (A $\text{Fe}_{1.2}\text{Cr}_{0.8}\text{O}_3$ Pigment), B (B YMnO_3), C(CE Fired) (Fired C $\text{Sr}_4\text{CuMn}_2\text{O}_9$ Pigment by CE Method), C(CO Fired) (Fired C $\text{Sr}_4\text{CuMn}_2\text{O}_9$ Pigment by CO Method), C(CO Dried) (Dried 110°C C $\text{Sr}_4\text{CuMn}_2\text{O}_9$ Pigment by CO Method)

	A	B	C(CE)	C(CO)	C(CO dried)	D	P25	Control
$t_{1/2}(\text{min})$	329	423	216	147	37	450	27	497
R^2	0.91	0.89	0.87	0.98	0.87	0.93	0.98	0.89

to reactor, A, B and D are the respective fired powders of pigment series and C(CE fired) is the fired C $\text{Sr}_4\text{CuMn}_2\text{O}_9$ pigment by CE method, C(CO fired) the fired C $\text{Sr}_4\text{CuMn}_2\text{O}_9$ pigment prepared by CO method and C(CO dried) is the dried (110°C) C $\text{Sr}_4\text{CuMn}_2\text{O}_9$ pigment prepared by CO method.

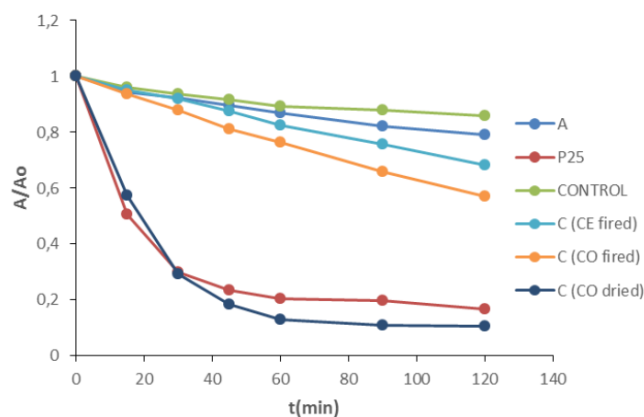


Figure 19: Photodegradation curves of Orange II with powders: P25 (Degussa reference), CONTROL (carried out without powder), A (A $\text{Fe}_{1.2}\text{Cr}_{0.8}\text{O}_3$ pigment), C(CE fired) (fired C $\text{Sr}_4\text{CuMn}_2\text{O}_9$ pigment by CE method), C(CO fired) (fired C $\text{Sr}_4\text{CuMn}_2\text{O}_9$ pigment by CO method), C(CO dried) (dried 110°C C $\text{Sr}_4\text{CuMn}_2\text{O}_9$ pigment by CO method).

The dry C $\text{Sr}_4\text{CuMn}_2\text{O}_9$ pigment prepared by CO method shows a photocatalytic activity against Orange II degradation similar to the P25 reference, but the fine powders are difficult to recover from the irradiated dispersion. The C fired CO powders ($1000^\circ\text{C}/6\text{h}$) shows a moderate photoactivity on Orange II with half time of 147 min lower than its homologous fired CE sample of C pigment ($1000^\circ\text{C}/12\text{h}$) with $t_{1/2}=216$ min. The A $\text{Fe}_{1.2}\text{Cr}_{0.8}\text{O}_3$ pigment show a low photoactivity over Orange II with $t_{1/2}=329$ min and finally both (B) YMnO_3 and (D) $\text{Sr}_2(\text{Mg}_{0.5}\text{Mn}_{0.5})\text{Ge}_2\text{O}_7$ pigments do not present significant photoactivity showing photodegradation half times similar to the CONTROL test. Pigment C that shows the highest photoactivity also presents the highest E_g (1.38 eV) of the pigment series; however the (A) $\text{Fe}_{1.2}\text{Cr}_{0.8}\text{O}_3$ pigment which shows the lowest E_g (1.13 eV) also presents some

photoactivity, therefore the photocatalytic activity is not associated directly to E_g ; other factors such as the e^- -hole pair recombination rate should be considered (Table 4) [40].

4. CONCLUSIONS

Cool black pigments whit interest for its application in asphalt urban pavements and building floors for moderate the urban heat island effect (UHI) based on (A) Cr doped hematite Fe_2O_3 (trigonal, $R-3c$), hexagonal perovskites (B) YMnO_3 (hexagonal, $P6_3cm$) and (C) $\text{Sr}_4\text{CuMn}_2\text{O}_9$ (trigonal, $P321$) and (D) melilite $\text{Mn-Sr}_2\text{MgGe}_2\text{O}_7$ (tetragonal, $P-42_1m$) with high NIR reflectance have been synthesized at optimized temperature-soaking time conditions showing the corresponding crystalline phase as the only phase at XRD.

(B) YMnO_3 pigment is the nearest black color to the carbon black used as reference, with $\Delta E^*=3.7$ followed by (D) $\text{Sr}_2(\text{MgMn})\text{Ge}_2\text{O}_7$ ($\Delta E^*=14.3$), (A) $\text{Fe}_{1.2}\text{Cr}_{0.8}\text{O}_3$ ($\Delta E^*=22.1$) and (C) $\text{Sr}_4\text{CuMn}_2\text{O}_9$ ($\Delta E^*=25.5$). The NIR diffuse reflectance R_{NIR} decreases in the sequence C (51%), B(39%), D (32%) and finally A(23%). E_g data measured from Kubelka Munk absorption spectra are into the range 1.38 eV for (C) $\text{Sr}_4\text{CuMn}_2\text{O}_9$ the nearest to ideal black bandgap to 1.13 eV for (A) $\text{Fe}_{1.2}\text{Cr}_{0.8}\text{O}_3$ pigment: the same progression that for R_{NIR} values.

Therefore, the pigment (C) $\text{Sr}_4\text{CuMn}_2\text{O}_9$ shows the nearest hue h to the reference carbon black and the highest NIR reflectance (51%). However the pigment (B) YMnO_3 shows the lowest color tolerance ΔE^* from the reference and the (A) $\text{Fe}_{1.2}\text{Cr}_{0.8}\text{O}_3$ pigment shows the minimum L^* and chroma C^* of the series (best black chroma).

Analysis of UV-Vis-NIR diffuse spectra indicates that a crystal field mechanism (CFM) of the chromophore ions Cr^{3+} and Fe^{3+} in corundum structure is associated to color of pigment A. Likewise a crystal field mechanism (CFM) explain the black color of

YMnO₃ associated to the D_{3h} trigonal bipyramid allowed transition of Mn³⁺ ions. A paired spin-exchange transition mechanism (PET) of Mn⁴⁺ ions with adjacent Mn⁴⁺ ions and also with adjacent Cu²⁺ explain the high intensity of absorption in the visible region for the pigment B and a probably intervalence charge transfer mechanism Mn³⁺- Mn²⁺ is involved to produce the color (IVCTM) in pigment D.

The pigments were applied in alkyd paint and two kind of glazes (double firing glaze at 1000°C and single firing glaze at 1080°C), and 2wt% added to porcelain stoneware powder (1200°C). The ceramic applications of (A) Fe_{1.2}Cr_{0.8}O₃ pigment shows good behavior in the free ZnO glaze and also in porcelain stoneware, (B) YMnO₃ and (C) Sr₄CuMn₂O₉ black pigments are compatible with low temperature glazes, and finally (D) Sr₂(Mg_{0.5}Mn_{0.5})Ge₂O₇ pigment loses the black color even in low temperature glazes application producing brown color. All pigments show high NIR reflectance in all tested applications.

In order to analyze the possible effect of stabilization of the pigment against the glazes, the (C) Sr₄CuMn₂O₉ pigment was prepared by ammonia coprecipitation method. However the fine particles of CO sample reacts with the glaze and decompose rapidly producing the profuse pin hole in the glazed sample.

The photoactivity of the pigment series on Orange II were estimated; the C Sr₄CuMn₂O₉ pigment shows moderate photoactivity on Orange II (t_{1/2}=216 min) and the A Fe_{1.2}Cr_{0.8}O₃ pigment also shows some activity (t_{1/2}=329 min), however both (B) YMnO₃ and (D) Sr₂(Mg_{0.5}Mn_{0.5})Ge₂O₇ pigments do not present significant photoactivity showing photodegradation half times similar to the CONTROL test. The photoactivity is not associated directly to E_g and other factors such as the e⁻-hole pair recombination rate should be considered.

ACKNOWLEDGEMENTS

The authors gratefully acknowledge the financial support of Universitat Jaume I (UJI B2018-43 Project).

REFERENCES

- [1] Monrós G, Scheelite and Zircon: Brightness, Color and NIR Reflectance in Ceramics, Nova Scienc Publishers, New York; 2021, ISBN: 978-1-53619-332-9
- [2] Akbari H, Levinson R. Evolution of Cool-Roof Standards in the US, *Advances in Building Energy Research*, 2008; 2: 1-32. <https://doi.org/10.3763/aber.2008.0201>
- [3] Taha H, Akbari H, Rosenfeld A, Huang J, Residential cooling loads and the urban heat island - the effects of albedo, *Building and Environment*, 1988; 23,4 : 271-283. [https://doi.org/10.1016/0360-1323\(88\)90033-9](https://doi.org/10.1016/0360-1323(88)90033-9)
- [4] Givoni B. *Climate considerations in building and urban design*. Van Nostrand Reinhold, New York; 1998.
- [5] CPMA Classification and chemical description of the complex inorganic color pigments, fourth ed. Alexandria, Dry Color Manufacturers Association, 2010.
- [6] Monrós G, Pigment Ceramic. in *Encyclopedia of Color Science and Technology*, Ronnier Luo ed., Springer; 2014. ISBN 978-1-4419-8070-0. ON LINE ISBN 978-3-642-27851-8 <http://www.springerreference.com/docs/html/chapterdbid/348055.html>.
- [7] Llusar M, Bermejo T, Primo JE, Gargori C, Esteve V, Monrós G. Karrooite green pigments doped with Co and Zn: Synthesis, color properties and stability in ceramic glazes. *Ceramics International*, 2017; 12,43: 9133-9144. <https://doi.org/10.1016/j.ceramint.2017.04.062>
- [8] ASTM C1371. Standard Test Method for Determination of Emittance of Materials Near Room Temperature Using Portable Emisometers, (2004).
- [9] Cerro S, Gargori C, Llusar M, Monrós G. Orthorhombic (Fe₂TiO₅)-monoclinic (Cr₂TiO₅) solid solution series: synthesis by gel routes, coloring and NIR reflectivity evaluation, *Ceramics International*, 2018; 44(11): 13349-13359. <https://doi.org/10.1016/j.ceramint.2018.04.167>
- [10] Gargori C, Cerro S, Fas N, Llusar M, Monrós G. Red-brown ceramic pigments based on chromium doped ferrian armalcolite, effect of mineralizers, *Ceramics International*, 2017; 43: 5490-5497. <https://doi.org/10.1016/j.ceramint.2017.01.065>
- [11] Gargori C, Cerro S, Fas N, Llusar M, Monrós G. Study of the photocatalytic activity and cool characteristics of a novel palette of pigments, *Boletín Sociedad Española Cerámica Vidrio*, 2017; 56: 166-176. <https://doi.org/10.1016/j.bsecv.2017.01.001>
- [12] Munsell AH. *Atlas of the Munsell color system*, Malden, Mass., Wadsworth, Howland & Co., inc., Printers, 1915. <https://doi.org/10.5479/sil.129262.39088002718880>
- [13] Molinari C, Conte S, Zanelli C, Ardit M, Cruciani G, Dondi M. Ceramic Pigments and Dyes beyond the Inkjet Revolution; from Technological Requirements to Constraints in Colorant Design, *Ceramics International*, 2020; 46(14): 21839-21872. <https://doi.org/10.1016/j.ceramint.2020.05.302>
- [14] Monrós G. Sol-Gel Materials for Pigments and Ceramics, *The Sol-Gel Handbook - Synthesis, Characterization and Applications Vol. 3*, ed. David Levy and Marcos Zayat, Wiley; 2015, ISBN 9783527334865. <https://doi.org/10.1002/9783527670819.ch37>
- [15] Boudjemaa A. Photo-catalytic hydrogen production over Fe₂O₃ based catalysts, *International Journal of Hydrogen Energy*, 2010; 35,15: 7684-7689. <https://doi.org/10.1016/j.ijhydene.2010.05.096>
- [16] Eppler RA. Cobalt-free black pigments, *American Ceramic Society Bulletin*, 1981; 61: 562-565.
- [17] Ozel M, Turan S. Production and Characterization of Iron-Chromium Pigments and Their Interactions with Transparent Glazes, *Journal of the European Ceramic Society*, 2003; 23(12): 2097-2104. [https://doi.org/10.1016/S0955-2219\(03\)00036-0](https://doi.org/10.1016/S0955-2219(03)00036-0)
- [18] Escardino A, Mestre S, Barba A, Beltrán V, Blasco A. Synthesis mechanism of an iron-chromium ceramic pigment, *Journal of the American Ceramic Society*, 2000; 83: 29-32. <https://doi.org/10.1111/j.1151-2916.2000.tb01143.x>
- [19] De Teresa JM, Ibarra MR, Algarabel PA, Ritter C. Evidence for magnetic polarons in the magnetoresistive perovskites,

- Nature, 1997; 386: 256-259.
<https://doi.org/10.1038/386256a0>
- [20] Smith AE, Mizoguchi H, Delaney K, Spaldin NA, Sleight AW, Subramanian MA. "Mn³⁺ in trigonal bipyramidal coordination: a new blue chromophore", *J Am Chem Soc*, 2009; 131: 17084-6.
<https://doi.org/10.1021/ja9080666>
- [21] Li J, Sleight AW, Subramanian MA. Determination of the Local Environment of Mn³⁺ and In³⁺ in the YInO₃-YMnO₃ Solid Solution, Which Exhibits an Intense Blue Color, *Chem Mater*, 2016; 28: 6050-6053.
<https://doi.org/10.1021/acs.chemmater.6b02827>
- [22] Abed AE, Gaudin E, Darriet J. Tetrastrontium dimanganese copper nonaoxide, Sr₄CuMn₂O₉. *Acta Cryst*, 2002; C58: i138-i140.
<https://doi.org/10.1107/S0108270102015639>
- [23] Abed EI, Gaudin E, Darriet J, Whangbo MH. Magnetic Susceptibility and Spin Exchange Interactions of the Hexagonal Perovskite-Type Oxides Sr₄/3(Mn₂/3Ni₁/3)O₃, *Journal of Solid State Chemistry*, 2002; 163: 513-518.
<https://doi.org/10.1006/jssc.2001.9439>
- [24] Byungseo B, Naoki T, Shinji T, Nobuhito I. Environmentally friendly orange pigments based on hexagonal perovskite-type compounds and their high NIR reflectivity, *Dyes and Pigments*, 2017; 147: 523-528.
<https://doi.org/10.1016/j.dyepig.2017.08.015>
- [25] Endo T, Doi Y, Hinatsu Y, Ohoyama K. Magnetic and Neutron Diffraction Study on Melilite-Type Oxides Sr₂MGe₂O₇ (M = Mn, Co), *Inorg Chem*, 2012; 51: 3572-3578.
<https://doi.org/10.1021/ic202386h>
- [26] Kim TG, Kim SJ, Lin CC, Liu RS, Chand TS, Ima SJ. Melilite-type blue chromophores based on Mn³⁺ in a trigonal-bipyramidal coordination induced by interstitial oxygen, *J Mater Chem*, 2013; C,1: 5843-5848.
<https://doi.org/10.1039/c3tc30795f>
- [27] CIE Commission International de l'Eclairage, Recommendations on Uniform Color Spaces, Colour Difference Equations, Psychometrics Colour Terms. Supplement n°2 of CIE Pub. N°15 (E1-1.31) 1971, Bureau Central de la CIE, Paris (1978).
<https://doi.org/10.1002/j.1520-6378.1977.tb00102.x>
- [28] Tauc J, Grigorovici R, Vancu A. Optical Properties and Electronic Structure of Amorphous Germanium, *Phys Status Solidi*, 1966; 15,2: 627-637.
<https://doi.org/10.1002/pssb.19660150224>
- [29] Kubelka P, and Munk F. Ein Beitrag Zur Optik Der Farbanstriche. *Z. Techn. Phys.*, 1931; 12: 593 -601.
- [30] Goldstein J. *Scanning Electron Microscopy and X-Ray Microanalysis*. Springer, 2003, ISBN 978-0-306-47292-3.
- [31] Konstantinou IK, Albanis TA. TiO₂-assisted photocatalytic degradation of azo dyes in aqueous solution: kinetic and mechanistic investigations. A review, *Applied Catalyst B: Environmental*, 2004; 49: 1-14.
<https://doi.org/10.1016/j.apcatb.2003.11.010>
- [32] Munsell AH, *Color Notation*. G.H Elis Company, 1905.
- [33] Schabbacha LM, Marinovski DL, Gütshb S, Bernardinc AM, Fredel MC. Pigmented glazed ceramic roof tiles in Brazil: Thermal and optical properties related to solar reflectance index, *Solar Energy*, 2018; 159: 113-124.
<https://doi.org/10.1016/j.solener.2017.10.076>
- [34] Cruciani G, Dondi M, Arditi A, Lyubenova TS, Carda JB, Matteucci F, Costa AL. Malayaite ceramic pigments: A combined optical spectroscopy and neutron/X-ray diffraction study, *Materials Research Bulletin*, 2009; 44: 1778-1785.
<https://doi.org/10.1016/j.materresbull.2009.03.006>
- [35] Vicent JB, Llusar M, Badenes J, Tena MA, Vicente M, Monrós G. Occlusion of chromophore oxides by Sol-Gel methods: Application to the synthesis of hematite-silica red pigments, *Boletín Sociedad Española Cerámica Vidrio*, 2000; 39,1: 83-93.
<https://doi.org/10.3989/cyv.2000.v39.i1.878>
- [36] Tanabe Y, Sugano S. On the absorption spectra of complex ions III, *Journal of the Physical Society of Japan*, 1956; 11: 864-877.
<https://doi.org/10.1143/JPSJ.11.864>
- [37] Pozza G, Ajò D, Chiari G, De Zuane F, Favaro M. Photoluminescence of the inorganic pigments Egyptian blue, Han blue and Han purple. *J Cult Heritage*, 2000; 1: 393-398.
[https://doi.org/10.1016/S1296-2074\(00\)01095-5](https://doi.org/10.1016/S1296-2074(00)01095-5)
- [38] Kendrick E, Kirk CJ, Dann SE. Structure and colour properties in the Egyptian Blue Family, M₁-xM'_xCuSi₄O₁₀, as a function of M, M' where M, M'=Ca, Sr and Ba. *Dyes Pigm*, 2007; 73: 13-18.
<https://doi.org/10.1016/j.dyepig.2005.10.006>
- [39] Shannon RD. Revised effective ionic radii and systematic studies of interatomic distances in halides and chalcogenides, *Acta Cryst*, 1976; A32: 751.
<https://doi.org/10.1107/S0567739476001551>
- [40] Czaja M, Lisiecki R, Chrobak A, Sitko R, Mazurak Z. The absorption- and luminescence spectra of Mn³⁺ in beryl and vesuvianite, *Physics and Chemistry of Minerals*, 2018; 45: 475-488.
<https://doi.org/10.1007/s00269-017-0934-x>
- [41] Weyl WA. *Coloured Glasses*. Dawson's of Pall Mall, London, 1959. <https://www.idesign.wiki/tag/glassmakers-soap/>
- [42] Ohtani B, Prieto-Mahaney OO, Lirabe D. What is Degussa (Evonik) P25? Crystalline composition analysis, reconstruction from isolated pure particles and photocatalytic activity test, *Journal of Photochemistry and Photobiology A: Chemistry*, 2010; 216(2-3): 179-182
<https://doi.org/10.1016/j.jphotochem.2010.07.024>
- [43] Shockley W. *Electrons and holes in semiconductors*, D. Van Nostrand Company, 1959.

Received on 27-04-2021

Accepted on 05-06-2021

Published on 01-07-2021

DOI: <https://doi.org/10.31875/2410-2199.2021.08.4>© 2021 Monrós *et al.*; Zeal Press.

This is an open access article licensed under the terms of the Creative Commons Attribution Non-Commercial License (<http://creativecommons.org/licenses/by-nc/3.0/>), which permits unrestricted, non-commercial use, distribution and reproduction in any medium, provided the work is properly cited.